Haptic Device Using a Newly Developed Redundant Parallel Mechanism

Arata, Jumpei
Department of Computer Science and Engineering, Graduate School of Engineering, Nagoya Institute of Technology

Kondo, Hiroyuki
Nagoya Institute of Technology

Ikedo, Norio
Nagoya Institute of Technology

Fujimoto, Hideo
Nagoya Institute of Technology

https://hdl.handle.net/2324/7168981

Haptic Device using a newly developed Redundant Parallel Mechanism

Jumpei Arata, *Member, IEEE*, Hiroyuki Kondo, Norio Ikedo and Hideo Fujimoto, *Member, IEEE*

Abstract—A number of haptic devices have recently become available on the commercial market, and these devices are becoming common not only in research but also in consumer use. In the present paper, a new parallel mechanism, referred to herein as DELTA-R (formerly referred to as DELTA-4) is proposed for a new haptic device having high-quality force display capability and operability. DELTA-R allows 3-DOF translational motions. The key features of DELTA-R, as compared with conventional parallel mechanisms, are redundant actuation, a smaller footprint, a larger working area, and improved access to the end-effector. The prototype is equipped with a 3-DOF rotation mechanism, the center of motion of which is located on the wrist position of the operator. An evaluation test of the force display was conducted using a prototype of the proposed mechanism. The present paper describes the kinematic design, kinematic modeling, kinematic analysis, prototype implementation, and evaluations.

Index Terms—Haptic device, Parallel mechanism, Kinematics, Force display device, Virtual reality.

I. INTRODUCTION

HAPTIC devices can be defined as devices that can display "a sense of touch" to the operator. This sense of touch can be described not only by a force, but also by vibrations, temperature, friction, and means (tactile senses). A number of studies have been conducted in this area, and several haptic devices with the capability of force display are commercially available. In force display devices, it is essential to realize different force sensations of soft/hard objects. In addition, smoothness and low inertia in unloaded motions are required for high-quality haptic sensation. Therefore, in terms of the structure of haptic devices, the following characteristics are preferable with respect to the quality of the force display.

- For displaying soft objects, high position resolution and high force resolution are required.
- For displaying hard objects, high stiffness and high output force are required.
- For smoothness and low inertia motions, high backdrivability and a lightweight end-effector are required.

These characteristics can be obtained by mechanical structures (position input - force output: impedance type haptic device) or compensated control methods with (a) force sensor(s) (force input - position output: admittance type haptic device). On the other hand, parallel mechanisms have been widely applied in the development of haptic devices. General parallel link manipulators can be defined as follows. *"A generalized parallel link manipulator is a closed-loop kinematic chain mechanism whose end-effector is linked to the base by several independent kinematic chains [1]"*. In general, parallel mechanisms are actuated by fixed actuators on the base part of the mechanism. Therefore, the study of parallel mechanisms is a rational approach to realizing the above characteristics in impedance type haptic devices. In the present paper, a new parallel mechanism, namely, DELTA-R (formerly referred to as DELTA-4) is proposed for a new haptic device having high-quality force display capability and operability. DELTA-R was developed in order to overcoming the limitation of a constrained working area, which is a common problem for haptic devices that use parallel mechanisms. Preliminary results on the proposed mechanism have presented in previous studies [36], [37]. The present paper investigates the advantages of the proposed mechanism as a haptic device.

II. RELATED RESEARCH

In general, haptic devices can be classified into two categories: impedance type devices and admittance type devices. In impedance type haptic devices, a high backdrivability of kinematics is required for smooth input motions. In admittance type haptic devices, although mechanical limitations are less restricted, a feedback control using (a) force sensor(s) is required. Therefore, in admittance type haptic devices, it is essential to deal with a force feedback control in terms of stability and quality of haptic sensation. Previously proposed haptic devices are listed in Table I along with the corresponding control type, mechanism, number of DOF of end-effector, references, and remarks.

A. Impedance type haptic devices

The PHANTOM (SensAble Technologies) [2] impedance type haptic device is widely applied in haptic research field. PHANTOM has a 6-DOF serial-parallel hybrid mechanism using a wire driven mechanism. Freedom 6S (MPB Technologies) [3] and Virtuose 6D35-45 (Haption) [4] have been developed as 6-DOF hybrid mechanism manipulators. CyberGrasp and CyberForce are exoskeleton haptic devices that are capable of displaying force on fingers developed by immersion [5].

In general, by using a serial link mechanism, it is possible to realize a larger working area. However, for the application of impedance type haptic devices, it is difficult to implement highly geared motors to realize high backdrivability. Consequently, it is difficult to realize high output force on impedance type haptic devices using serial link mechanisms. To solve this

J. Arata is with the Department of Computer Science and Engineering, Graduate School of Engineering, Nagoya Institute of Technology, Gokiso-cho, Showa-ku, Nagoya 466-8555, JAPAN, e-mail: jumpei@nitech.ac.jp.

H. Kondo, N. Ikedo and H. Fujimoto are with Nagoya Institute of Technology.

TABLE I
MECHANICAL FEATURES OF HAPTIC DEVICES

Device	Type / Mechanism	DOF of end-effector	Ref.	Remark
Phantom Premium 6 DOF	Impedance / Hybrid	3 trans. + 3 rot.	[2]	A parallelogram
Freedom 6S	Impedance / Hybrid	3 trans. + 3 rot.	[3]	A parallelogram + 3 DOF wire mechanism
Cubic 3	Impedance / Parallel	3 trans.	[3]	3 DOF parallel mechanism
Virtuose 6D Desktop	Impedance / Parallel	3 trans. + 3 rot.	[4]	6 DOF parallel mechanism
Virtuose 6D35-45	Impedance / Hybrid	3 trans. + 3 rot.	[4]	2 parallelograms
CyberGrasp	Impedance / Hybrid	5 (1 par a finger)	[5]	Link and Wire mechanism
CyberForce	Impedance / Hybrid	3 trans. + 3 rot.	[5]	A parallelogram
DELTA	Impedance / Parallel	3 trans.	[6]	DELTA parallel mechanism
Omega.3/6/7	Impedance / Parallel	3 trans. + 3 rot. + 1 grasp	[8]	Based on DELTA[6] parallel mechanism
Novint Falcon	Impedance / Parallel	3 trans.	[9]	Based on DELTA[6] parallel mechanism
Haptic Master	Impedance / Parallel	3 trans. + 3 rot.	[10]	Redundant parallel mechanism
Pen-based force display	Impedance / Parallel	3 trans. + 3 rot.	[11]	2 set of 3 DOF manipulators
3-DOF Planar Pantograph	Impedance / Parallel	2 trans. + 1 rot.	[12]	2 pantographs
5-DOF Haptic Wand	Impedance / Parallel	3 trans. + 2 rot. + 1 passive rot.	[12]	Using a dual-pantograph arrangement
ShaDe	Impedance / Parallel	3 rot.	[15]	Based on Agile Eye spherical mechanism
Pantoscope	Impedance / Parallel	2 rot.	[16]	2 DOF spherical mechanism
Xitact IHP/ITP	Impedance / Parallel	3 rot. + 1 linear	[17]	Based on Pantoscope[16]
3 DOF parallel hand	Impedance / Parallel	3 trans.	[18]	10-Link, 12 revolute-joint mechanism
6 DOF haptic device	Impedance / Hybrid	3 trans. + 3 rot.	[19]	Orthoglide + Agile Eye
SPIDAR	Impedance / Wire	3 trans. + 3 passive rot.	[20]	Wire mechanism
Mimic Mantri	Impedance / Wire	3 trans. + 3 passive rot.	[22]	Wire mechanism
Master robot using a radial wire	Impedance / Wire	3 trans. + 3 rot.	[23]	Wire mechanism
Excalibur	Impedance / Wire	3 trans.	[24]	Using a patented steel cable
WireMan	Impedance / Wire	3 trans.	[25]	Wire mechanism
HapticGEAR	Impedance / Wire	3 trans.	[26]	Wire mechanism
r^3-system	Impedance / Wire	1 trans.	[27]	Wire mechanism
HapticMASTER	Admittance / Serial	3 trans.	[28]	Cylindrical coordinate type mechanism
VISHARD6	Admittance / Serial	3 trans. + 3 rot.	[29]	SCARA 3 DOF + 3 DOF of rotation
VISHARD10	Admittance / Serial	3 trans. + 3 rot.	[30]	10 DOF hyper-redundant mechanism
Compact 6-DOF Haptic Interface	Admittance / Hybrid	3 trans. + 3 rot.	[31]	Modified DELTA [32] + gimbal [33]
DELTA-R	Impedance / Parallel	3 trans.	-	DELTA-R redundant parallel mechanism

problem, parallel mechanisms have been applied to impedance type haptic devices. By using parallel mechanisms, it is possible to realize high backdrivability, high stiffness, high output force, and low inertia. However, most parallel mechanisms have a disadvantage with respect to the working area. Clavel developed a 3-DOF parallel mechanism called DELTA [6]. Omega (Force Dimension) [8] is an application of the DELTA parallel mechanism as a haptic device. The DELTA mechanism was also applied to Novint Falcon (Novint Technologies) [9]. Iwata et al. developed a 6-DOF redundant parallel mechanism for a larger working area [10]. Iwata et al. developed a pen-based force display device [11]. Birglen et al. developed the ShaDe system [15], and Clavel et al. developed Pantoscope [16], which realizes 2-DOF rotational motions. The pantoscope has been implemented as a surgical simulator, Xitact IHP/ITP [17]. These rotational parallel mechanisms realize a remote center of motion (RCM) in space. Adelstein et al. developed a 3-DOF joystick type force display device using a 10-link "in-parallel" mechanism [18]. Chablet et al. developed a 6-DOF haptic device using Orthoglide within translational 3-DOF motion and Agile eye within a rotational 3-DOF parallel mechanism [19].

In addition, a number of wire-driven parallel mechanisms have been introduced in haptic research field as impedance type haptic devices. In SPIDAR [20] (CyVerse [21]) and Mimic Mantri [22] (Mimic Technologies), several strings are attached to the end-effector, and the string tension is controlled by motors for displaying force. A master robot using a radial wire-driven system [23] that uses seven wires has been developed in order to optimize the number of wires

needed for a 6-DOF haptic device. Excalibur [24] is a 3-DOF translational haptic device using a wire-driven parallel mechanism. This mechanism has been developed for versatile applications, including a virtual reality (VR) training system and computer aided design (CAD). WireMan[25] is a wearable force display device that is actuated by parallel wires and has been developed in order to investigate the possibility of creating aids for blind people. HapticGEAR [26] is also a wearable force display device that has been developed in order to provide haptic sensation in a large VR space generated by an immersive visual display. The r^3-system has been developed for use in sport simulation in a large VR space. The r^3-system was designed to realize highly dynamic sport simulations (e.g., a rowing simulator and a tennis training system).

B. Admittance type haptic devices

HapticMASTER [28] (Moog FCS Robotics) and VISHARD10[30] (Ueberle et al.) have been presented as admittance type haptic devices. These devices use serial link mechanisms. Using a parallel mechanism, Uchiyama et al. developed Modified DELTA[31] along with a five-link parallel gimbal mechanism.

III. KINEMATICS

An overview of the developed DELTA-R structure is shown in Fig. 1. DELTA-R incorporates a new parallel mechanism, which realizes translational 3-DOF motions.
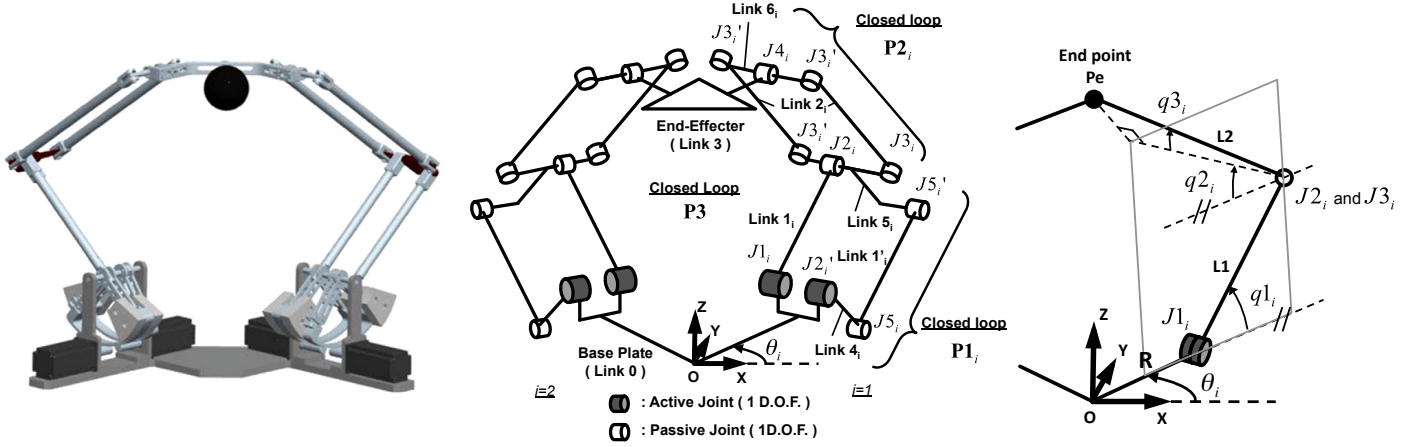
Fig. 1. Overview of the DELTA-R mechanism that realizes translational 3-DOF motions by four fixed motors on the base (left). The structure of DELTA-R consists of a base plate, an end-effector, and two arms. Each arm consists of two parallelograms $P1_i$ and $P2_i$ (center). Each arm can be modeled by introducing angle parameters $q1_i$, $q2_i$, and $q3_i$ (right).

A. Mechanism

DELTA-R is a redundant parallel mechanism that realizes translational 3-DOF motions by four fixed actuators on the base plate. The structure of DELTA-R is illustrated in Fig. 1. The kinematics of DELTA-R consists of a base plate, an end-effector, and a pair of arms. Each arm consists of two parallelograms ($P1_i$ and $P2_i$). (The suffix $i = 1, 2$ represents a pair of arms.) Link 5 is a T shape linkage bar, which connects parallelograms $P1_i$ and $P2_i$ in each arm. The motors attached to joints $J1_i$ and $J2_i'$ in each arm enable 2-DOF motions. Two arms are fixed on the base plate at allocation angle θ_i from the X axis around the Z axis of the reference frame O. End-effectors are attached to the tips of the two arms by joint $J4_i$ of parallelogram $P2_i$. The connections between the end-effectors and the two parallelograms by $J4_i$ gives the motion constraint in parallel between the end-effector and the base plate. By introducing this motion constraint, it is possible to maintain the posture between the end-effector and the base plate in parallel, and the DELTA-R can finally obtain the translational 3-DOF motions by means of its redundant mechanism.

The name of the DELTA-R mechanism was derived from the conventional DELTA parallel mechanism, because there are several common points on the motion constraints of the end-effectors, and -R refers to the redundant mechanism. By the implementation of a new redundant parallel mechanism, the following benefits can be obtained in DELTA-R: a larger working area, a smaller footprint, and improved mechanical access of the end-effectors.

B. Geometric parameters and definitions

In the kinematics of DELTA-R, the geometric solutions can be given both in the forward kinematics and the inverse kinematics. The lengths of Links 0, 1, 2, and 3 in Fig. 1 are denoted as $L0$, $L1$, $L2$, and $L3$, respectively. The rotation angles around $J1_i$, $J2_i$, and $J3_i$ are denoted as $q1_i$, $q2_i$, and $q3_i$, respectively. The joint angles of $J2_i$ and $J2_i'$ are equivalent, based on parallelogram $P1_i$. In these joints, angles

$q1_i$ and $q2_i$ can be measured by position sensors (such as optical encoders) attached to the actuators. Using these parameters, the kinematics of DELTA-R can be simplified and are described in Fig. 1. The length R in Fig. 1 can then be given as follows:

$$R = L0 - L3. \tag{1}$$

C. Forward kinematics

The end-effector position $\mathbf{P}e_i = (px_i\, py_i\, pz_i)^T$ can be obtained from joint angles $q1_i$, $q2_i$ of $J1_i$, and $J2_i$ based on the forward kinematics.

$$
\begin{aligned}
{}^0\mathbf{T}_{ei} = \ & Rot(\mathbf{Z}, \theta i)Trans(R, 0, 0)Rot(\mathbf{Y}, -q1_i) \\
& Trans(L1, 0, 0)Rot(\mathbf{Y}, q1_i + q2_i) \\
& Trans(-L2cos(q3_i), L2sin(q3), 0).
\end{aligned} \tag{2}
$$

The translation vector in ${}^0\mathbf{T}_{ei}$ is equivalent to the end-effector position $\mathbf{P}e_i$. Therefore, $\mathbf{P}e_i$ can be given as follows:

$$
\begin{pmatrix} px_i \\ py_i \\ pz_i \end{pmatrix} = \begin{pmatrix} A_i - C_iC_{3i} - L2S_{3i}S_{\theta i} \\ B_i - D_iC_{3i} + L2S_{3i}C_{\theta i} \\ L1S_{1i} + L2C_{3i}S_{2i} \end{pmatrix}, \tag{3}
$$

where

$$
\begin{aligned}
j \ &= 1, 2, 3, \\
A_i \ &= (R + L1C_{1i})C_{\theta i}, \quad B_i = (R + L1C_{1i})S_{\theta i}, \\
C_i \ &= L2C_{2i}C_{\theta i}, \quad D_i = L2C_{2i}S_{\theta i}, \\
C_{ji} \ &= \cos(qj_i), \quad S_{ji} = \sin(qj_i), \\
C_{\theta i} \ &= \cos(\theta_i), \quad S_{\theta i} = \sin(\theta_i).
\end{aligned}
$$

The angle $q3_i$ of a passive joint can be obtained by active joint angles from Equation (3) as simultaneous equations of $\mathbf{P}e_1 = \mathbf{P}e_2$. Therefore, $q3_i$ can be obtained as follows:

$$q3_i = 2\arctan(u_i), \tag{4}$$

$$u_i = \frac{-G_i \pm \sqrt{G_i^2 - 4H_iI_i}}{2H_i}, \tag{5}$$

$$E_i = L1S_{11} - L1S_{12} - L2C_{2i},$$

$$F_i = L1S_{11} - L1S_{12} + L2C_{2i},$$

$$G_1 = -2L2^2(C_{\theta 1}S_{\theta 2} - S_{\theta 1}C_{\theta 2})S_{22},$$

$$G_2 = -2L2^2(C_{\theta 1}S_{\theta 2} - S_{\theta 1}C_{\theta 2})S_{21},$$

$$H_1 = ((B_1 - B_2 + D_1)L2S_{22} + D_2E_1)S_{\theta 2}$$
$$+ ((A_1 - A_2 + C_1)L2S_{22} + C_2E_1)C_{\theta 2},$$

$$H_2 = ((B_1 - B_2 - D_2)L2S_{21} + D_1F_2)S_{\theta 1}$$
$$+ ((A_1 - A_2 - C_2)L2S_{21} + C_1F_2)C_{\theta 1},$$

$$I_1 = ((B_1 - B_2 - D_1)L2S_{22} + D_2F_1)S_{\theta 2}$$
$$+ ((A_1 - A_2 - C_1)L2S_{22} + C_2F_1)C_{\theta 2},$$

$$I_2 = ((B_1 - B_2 + D_2)L2S_{21} + D_1E_2)S_{\theta 1}$$
$$+ ((A_1 - A_2 + C_2)L2S_{21} + C_1E_2)C_{\theta 1},$$

where u_i is an intervening variable. Based on the geometric conditions, u_i in Equation (5) should have a negative value.

Therefore, the angle $q3_i$ of a passive joint is obtained as above. By adding $q3_i$ to Equation (3), the end-effector position Pe is eventually obtained.

D. Inverse kinematics

The joint angles $q1_i$ and $q2_i$ of $J1_i$ and $J2_i$, respectively, can be given in term of the end-effector position Pe using the inverse kinematics of DELTA-R. First, the position of joint $J2_i$, $\mathbf{P}_{J2i} = [J2x_i, J2y_i, J2z_i]^T$, can be denoted as follows:

$$^0\mathbf{T}_3 = Rot(Z_0, \theta i)Trans(R, 0, 0) \tag{6}$$
$$Rot(Y_2, -q1_i)Trans(L1, 0, 0)$$
$$= \left[\begin{array}{c|c} ^0\mathbf{E}_3 & ^0\mathbf{P}_3 \\ \hline \mathbf{0} & 1 \end{array} \right]. \tag{7}$$

because $^0\mathbf{P}_{3i} = \mathbf{P}_{J2i}$, $\mathbf{P}_{J2i}$ can be obtained as

$$^0\mathbf{P}_{3i} = \mathbf{P}_{J2i} = \left[\begin{array}{c} J2x_i \\ J2y_i \\ J2z_i \end{array} \right] = \left[\begin{array}{c} (R + L1C_{1i})C_{\theta i} \\ (R + L1C_{1i})S_{\theta i} \\ L1S_{1i} \end{array} \right] \tag{8}$$

Then, joint $J2_i$ can also be determined as points on a sphere centered at end-effector position Pe with a radius of $L2$:

$$(Jx_i - px)^2 + (Jy_i - py)^2 + (Jz_i - pz)^2 = L2^2. \tag{9}$$

By introducing an intervening variable s_i, $q1_i$ can be obtained from Equation (9), as follows:

$$q1_i = 2\arctan(s_i), \tag{10}$$

$$s_i = \frac{2pz \pm \sqrt{4pz^2 - M_iN_i}}{M_i}, \tag{11}$$

$$K_i = 2C_{\theta i}px + 2S_{\theta i}py,$$

$$L = \frac{1}{L1}(L1^2 - L2^2 + R^2 + px^2 + py^2 + pz^2),$$

$$M_i = L - 2R + (1 - \frac{R}{L1})K_i,$$

$$N_i = L + 2R - (1 - \frac{R}{L1})K_i.$$

From the geometric conditions, s_i in Equation (11) should have a negative value. The projection of the trajectory of Link 2 onto the XY plane can be described as an ellipsoid having major axis $L2$ and minor axis $L2C_{2_i}$. Therefore, $q2_i$ is obtained as follows:

$$px'_i = pxC_{\theta i} + pyS_{\theta i},$$

$$py'_i = pyC_{\theta i} - pxS_{\theta i},$$

$$q2_i = \arccos\left(\sqrt{\frac{(px'_i - (R + L1C_{1i}))^2}{L2^2 - py'_i}} \right). \tag{12}$$

Based on the above equations, the joint angles $q1_i$ and $q2_i$ of $J1_i$ and $J2_i$, respectively, can be obtained. The kinematics, including the Jacobian, is described in greater detail in the Appendix.

E. Singularity point

In the DELTA-R mechanism, there are reduced mobility points for the case in which the parallelograms $P1_i$ and $P2_i$ are aligned on the same plane or in which $P2_i$ is aligned on the same plane as the base plate. These singularity points can be easily avoided by placing mechanical stoppers on joints $J1_i$ and $J2_i$. In addition, there are additional singularity points at which the alignment angle between the two arms, $\theta_2 - \theta_1$, is 0 or 180 deg. However, this angle is fixed on the base, and so these singularity points can be eliminated during the design process. The optimal value of $\theta_2 - \theta_1$ in terms of manipulability is 90 deg. On the other hand, in the DELTA mechanism, there is an over mobility point for the case in which the all three upper parallelograms are aligned in parallel. However, there is no over mobility point in the DELTA-R mechanism.

IV. ANALYSIS

DELTA-R incorporates two arms and a redundant mechanism. Therefore, compared with the conventional DELTA parallel mechanism (three arms), DELTA-R has advantages with respect to working area and footprint. The basic structures of DELTA and DELTA-R are shown in the top panels of Fig. 2. For comparison of the footprints and working volumes, the conditions of the mechanisms (such as the link lengths and angle ranges) are configured identically based on the prototype implementation parameters of DELTA-R. Comparing these mechanisms, DELTA-R has a 15% larger working area and a 40% smaller footprint for installation (middle panels of Fig. 2). In addition, DELTA-R enables operators to effectively access a large working area by aligning the arms and actuators in a V shape. The motion traces on XY plane of DELTA-R and DELTA structure on 12 representative points around the center of working area are shown in the bottom panels of Fig. 2. The figure clearly shows that improved access to the
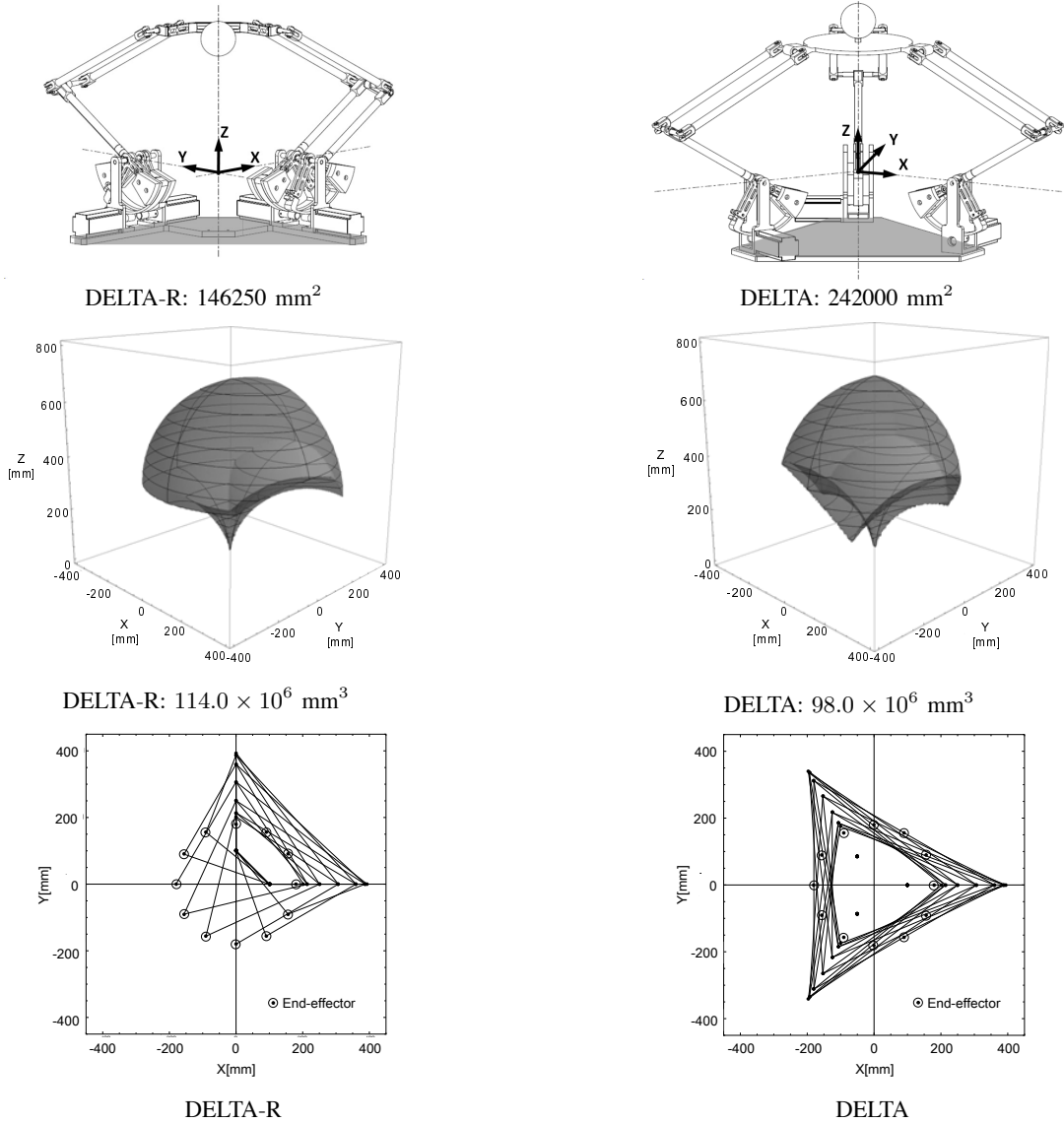
Fig. 2. A comparison of the footprints of DELTA-R and DELTA in the same mechanical configurations revealed that DELTA-R realizes a 40% smaller footprint (top panels). A comparison of the working areas of DELTA-R and DELTA in the same mechanical configurations revealed that DELTA-R realizes a 15% larger working area (middle panels). The lines and dots show the motion trace of the structure, of the mechanisms on XY plane. DELTA-R enables operators to effectively access the working area by aligning the arms and actuators in a V shape (top panels). The average footprint of the structure in 12 representative points is two times smaller in DELTA-R compared with DELTA (bottom panels).

device from users by the two-arm configuration of DELTA-R. In addition, the average footprint area of structure on these points are 59170 mm^2 and 115857 mm^2, in DELTA-R and DELTA respectively. Therefore, the footprint area of structure in motions are roughly two times smaller in DELTA-R compared to DELTA.

Force producibility indicates how easily a force can be produced in a given direction. In the general parallel mechanism, force producibility varies depending the end-effector position. Therefore, observing the force producibility by kinematic analysis is useful for examining the performance of the different mechanisms. In this section, the force producibilities of DELTA-R and DELTA are compared. First, the motor torque τ can be obtained by Equation (13) using the Jacobian $\mathbf{J}$ and the force vector $\mathbf{F}$. The Jacobian $\mathbf{J}$ is given by the end-effector position, and the force vector $\mathbf{F}$ is given by Equation (17).

$$\tau = \mathbf{J}^T \mathbf{F}, \tag{13}$$

$$\mathbf{F} = \begin{bmatrix} F_x & F_y & F_z \end{bmatrix}^T, \tag{14}$$

$$F_x = Fn \sin\theta \cos\varphi, \tag{15}$$

$$F_y = Fn \sin\theta \sin\varphi, \tag{16}$$

$$F_z = Fn \cos\theta. \tag{17}$$

where θ and φ are Eulerian coordinates parameters, and Fn is the norm of $\mathbf{F}$. Then, the extremal forces can be obtained as the maximum Fn, where the motor torque τ does not exceed the rated motor torque τ_{lim}. In this analysis, an SGMJV-ADA motor (Yasukawa Electric Corporation, Japan, Rated torque: 1.27 Nm) was chosen, that was implemented in the prototype, as described in Section V. The extremal forces were calculated
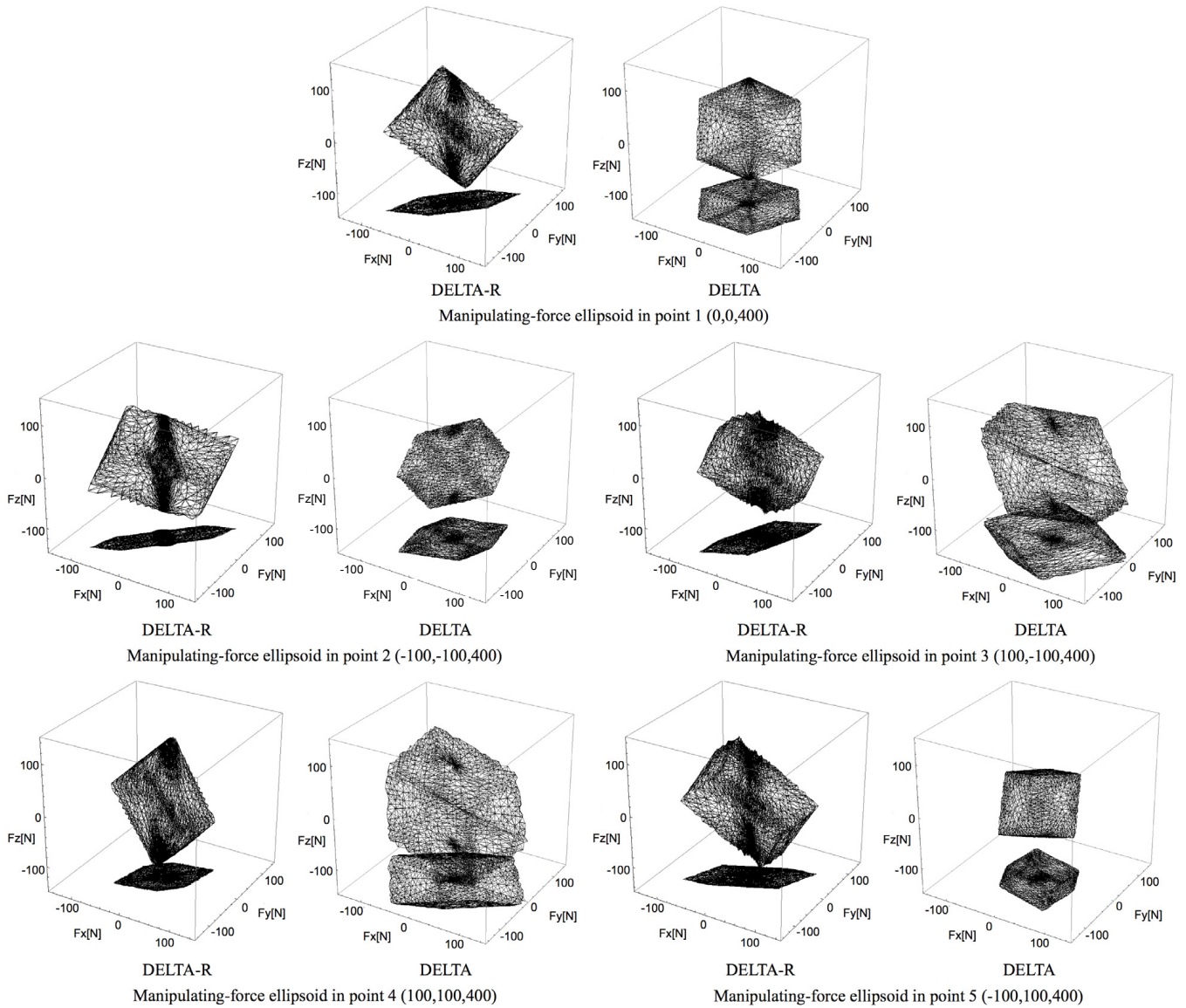
Fig. 3.   Force producibility analysis: extremal forces of DELTA-R and DELTA at five points, labeled 1 through 5, over the working area: 1 (0, 0, 400), 2 (-100, -100, 400), 3 (100, -100, 400), 4 (100, 100, 400), and 5 (-100, 100, 400).

in all directions at five representative points over the working area, namely, Point 1 (0, 0, 400), Point 2 (-100, -100, 400), Point 3 (100, -100, 400), Point 4 (100, 100, 400), and Point 5 (-100, 100, 400). The results of the analysis are illustrated in Fig. 3.

Compared to DELTA, the force producibility of DELTA-R is elongated in the X-Y plane. This means that, for DELTA-R, it may be difficult to provide adequate force depending on the output force direction (especially in the X and Y directions). In DELTA, three arms are located evenly at intervals of $120 \deg$. In DELTA-R, a pair of arms are located at angles of $\theta_2 - \theta_1$. Therefore, the evenly distributed DELTA kinematic structure has an advantage with respect to force producibility. In addition, in DELTA-R, the force producibility was shown to deteriorate when X and Y values are negative (Point 2). The angle between the links of the $J4$-end-effector of

each arm, θ_A, is strongly related to the deterioration of the force producibility. As shown in Fig. 4, θ_A becomes smaller with increasing distance from the original position when the X and Y values are negative. In DELTA-R, the XYZ translational force is generated by two arms. Therefore, the force producibility decreases as the planes of the two arms become closer. This analysis reveals the advantage of the evenly distributed DELTA mechanism, as compared to that of DELTA-R. However, DELTA-R has an advantage with respect to the working area distribution. As mentioned above, by aligning the arms and motors in a V shape, DELTA-R enables the operator to effectively access a large working area. Thus, this is a design trade-off of the kinematic structures. On the other hand, in the kinematics of both DELTA and DELTA-R, all of the motors can be situated on the base plate. Therefore, in terms of design, the actuator limitations with respect to
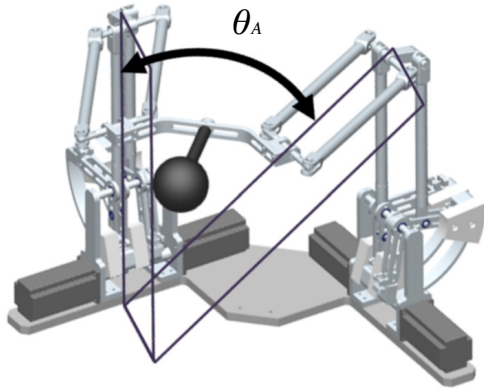
Fig. 4. In DELTA-R, the XYZ translational force is generated by two arms. Therefore, the force producibility decreases as the planes of the two arms become closer.

size and weight are not crucial. Thus, the advantages of the DELTA-R mechanism, i.e., an improved mechanical access of the end-effectors can be exploited by introducing an adequate mechanical design.

V. IMPLEMENTATION

A. Realization of the DELTA-R mechanism

Figure 5 shows the implemented prototype of DELTA-R. The link parameters $L0$, $L1$, $L2$, and $L3$ are given as $300, 300, 400,$ and 200 mm, respectively. The angular ranges of motion are $q1_i$: 0 to 90 deg, $q2_i$: 5 to 90 deg, and $q3_i$: -70 to 70 deg. In considering the usability and the working area, the arm angles were set to $\theta_1 = 0$ deg and $\theta_2 = 90$ deg (90 deg between arms).

In order to realize high backdrivability, four direct AC servo motors and a wire reduction mechanism were incorporated into the prototype. In the wire reduction mechanism, counterweights were attached in order to compensate for gravity. Tables II and III show the specifications of the prototype. In the impedance type haptic device, mechanical backlash and play significantly decrease performance, and commonly used reduction gears are not suitable for such devices. Therefore, we implemented a wire reduction system, as shown in Fig. 5. The reduction ratio is 14:1. A pulley was connected to the motor shaft using stainless steel wire (diameter: 1.0 mm, winding: 7 x 7). The wire was wound around the motor shaft four times based on Euler's belt theory (maximum torque transmission: 18.8 Nm). Counterweights were attached in order to compensate for gravity, and mechanical stoppers were implemented in order to prevent singularities.

A 3-DOF rotation mechanism and a grasping mechanism were attached to the prototype. Therefore, the prototype has a total of seven DOF (3-DOF translation, 3-DOF rotation, and 1-DOF grasping). In the prototype, the required working area was given by the standard working volume of the human arms from a seated position. Therefore, based on a numerical analysis, the prototype link parameters, such as the link lengths $L1$ and $L2$, are defined so as to maximize the working volume. For the case in which $L2 = R + L1$, the working volume can be maximized.
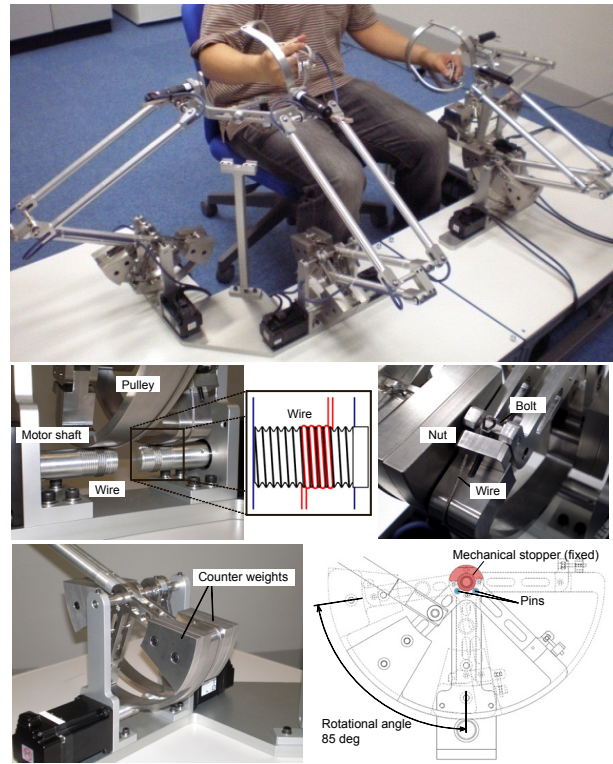
Fig. 5. In order to realize high backdrivability, four direct AC servo motors and a wire reduction mechanism are incorporated into the prototype (top). A wire reduction system was implemented in order to realize high backdrivability (middle). Counterweights are attached in order to compensate for gravity, and mechanical stoppers are implemented in order to prevent singularities (bottom).
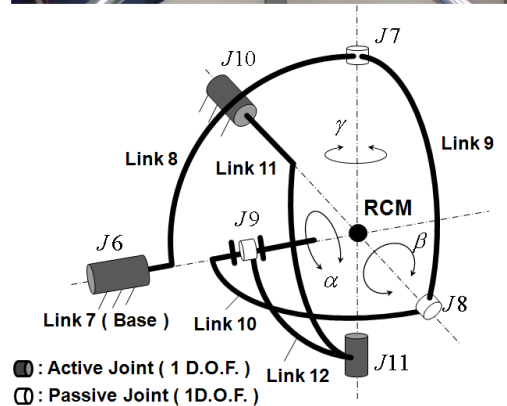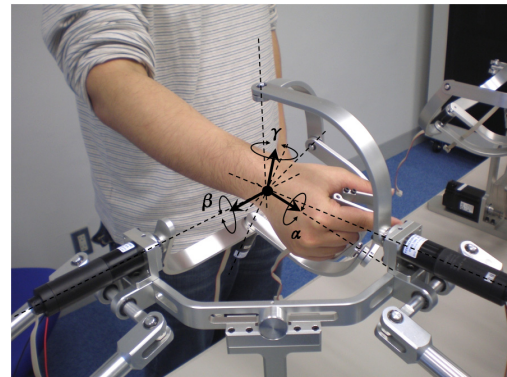
Fig. 6. A 3-DOF rotation mechanism is implemented by extending the 2-DOF five-spherical-link mechanism proposed by Ouerfelli et al. [33]. An actuator for grasping motion is attached to the end-effector of the 3-DOF rotation mechanism.

TABLE II
MECHANICAL SPECIFICATIONS OF THE DELTA-R PROTOTYPE

Working area	translation $\phi 500 \times$ L200 mm
	rotation $\pm 80 \times \pm 80 \times \pm 80$ deg
Output force	Continuous 50 N in X, Y and Z axes
Resolutions	Liner 0.01 mm
	angler 0.01 deg
Dimension	Height 500 mm
	Width 800 mm
	Depth 800 mm

TABLE III
SPECIFICATIONS OF THE MOTOR USED IN THE PROTOTYPE

Joint	$J1_i, J2_j^{(a)}$	$J6, J10^{(b)}$	$J11$,Grasping$^{(c)}$
Rated Power [W]	400	47.9	8.68
Rated Torque [Nm]	1.27	44×10^{-3}	10×10^{-3}
Rated Rev [rpm]	3000	6000	8000
Gear ratio	-	16:1	28:1
Resolution	2^{20}	512	512

(a) SGMJV-ADA(Yasukawa Electric Corporation, Japan)
(b) 2657W024CR(Faulhaber, Germany)
(c) 2232A024SR(Faulhaber, Germany)

TABLE IV
COMPARISON BETWEEN DELTA-R AND DELTA

	DELTA-R	DELTA
Footprint	146,250 mm^2	242,000 mm^2
Working area	114.0×10^6 mm^3	98.0×10^6 mm^3

B. Rotation and grasping mechanism

The developed 3-DOF rotation mechanism and its kinematics model are shown in Fig. 6. The 3-DOF rotation mechanism is implemented by extending the 2-DOF five-spherical-link mechanism proposed by Ouerfelli et al. [33]. An actuator for grasping motion is attached to the end-effector of the 3-DOF rotation mechanism.

In the 3-DOF rotation mechanism, two of the three active joints ($J10$, $J6$) are fixed to the base. All of the centers of rotation are fixed at a point (RCM). The 3-DOF rotation mechanism was designed for smooth input motion from an operator. Therefore, the RCM corresponds to the wrist joint of the operator when he/she handles the grasping part. The distance between the grasping part and the RCM is decided based on a standard human body.

The weight of the rotation mechanism, including all motors, is 1.5 kg. In this prototype, the gravity was compensated by counterweights on the base. Approximately 50 % of the gravity is compensated the counterweights (passive) and the rest is compensated by motors (active) for decreasing the effect of inertia.

VI. EVALUATION

In order to test the performance of the prototype as a haptic device, a force display test, stiffness measurement, and resistance force measurement were performed. In addition, a virtual sphere was displayed in order to test the overall performance of the prototype as a haptic device. In these experiments, the device was controlled by VxWorks 5.5.1 at a control frequency of 1 kHz.

A. Force display test

For impedance type haptic devices, it is important to output a desired force value without having a force feedback sensor. An experiment was conducted to test the accuracy of the output force. In this experiment, the generated force was calculated only by the kinematic model and the measured force was not fed back to the controller.

1) Experimental setup: The output force was measured at five points, namely, Point 1 (0, 0, 400), Point 2 (-100,-100,400), Point 3 (100,-100,400), Point 4 (100,100,400), and Point 5 (-100,100,400), in the reference frame O. The output force was varied from 0 to 10 N in 2 N increments on the X, Y, and Z directions. A six-axis force sensor (Nitta Corporation, IFS-50M31A25-I25) was positioned at each point by a sensor jig (top of Fig. 7).

2) Experimental results: Representative experimental results (Point 1) are shown in the bottom panel of Fig. 7. The experimental results reveal that the force was displayed with average error 0.15 N (maximum error: 0.3 N) in each direction. However, crosstalk was observed to be approximately 0.5 N in the measurements in the X and Y directions. Crosstalk in the Z direction was not strongly observed (0.27 N). The mobility of the mechanism should be considered as a possible reason for this phenomenon. In the DELTA-R structure, it is necessary to take into account the resultant force of the two arms in order to generate the force on the XY plane. In this case, one arm should bend passively. Consequently, the effect of distortion of the mechanical structure increases. Therefore, crosstalk was smaller in the Z direction. This can also be explained by force producibility analysis. The force producibility of DELTA-R is elongated in the XY plane.

B. Stiffness measurement

In this experiment, the stiffness of the prototype was measured by applying a static load in the X, Y, and Z directions.

1) Experimental setup: The top panel of Fig. 8 shows an overview of the experimental setup. The end-effector was fixed at the center of the working area (Point 1 on the force display test) by fixing all active joints during the measurement. The load was gradually increased from 2 N to 11 N in 3 N increments. In a similar manner, the load was then gradually unloaded in 3 N increments in the X, Y, and Z directions. An Optotrak Certus motion capture system (Northern Digital Inc.) [34] was used for position measurement by placing optical markers on the prototype. The RMS positional accuracy and resolution of the Optotrak are 0.1 mm and 0.01 mm, respectively. The sampling rate was set to 100 Hz, and position measurement was conducted for 5 second under each condition. Although the wire transmission mechanism was incorporated into the prototype, the mechanical parameters of mechanism were not identified (e.g., elasticity) or implemented in the control system for this test.

2) Experimental results: The experimental results are shown in the bottom panel of Fig. 8. The points on the graph represent the average of 5 second of measurement at 100 Hz. The range of the mean error was less than 0.02 mm. The experimental results revealed that the stiffnesses
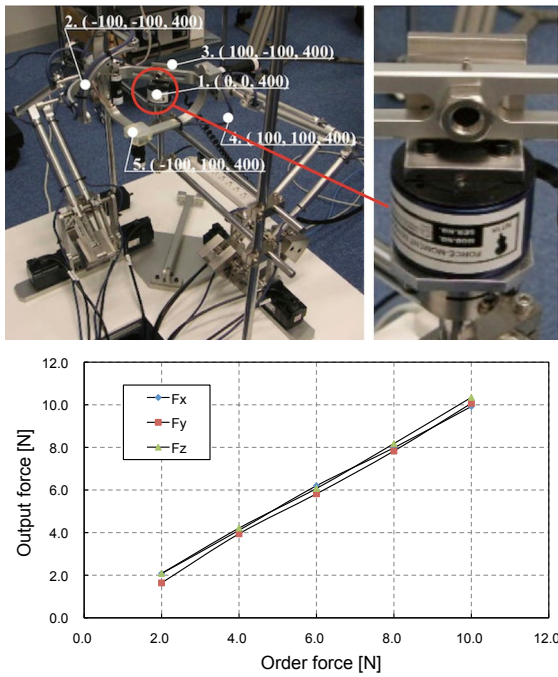
Fig. 7.   Experimental setup and results of the force display test
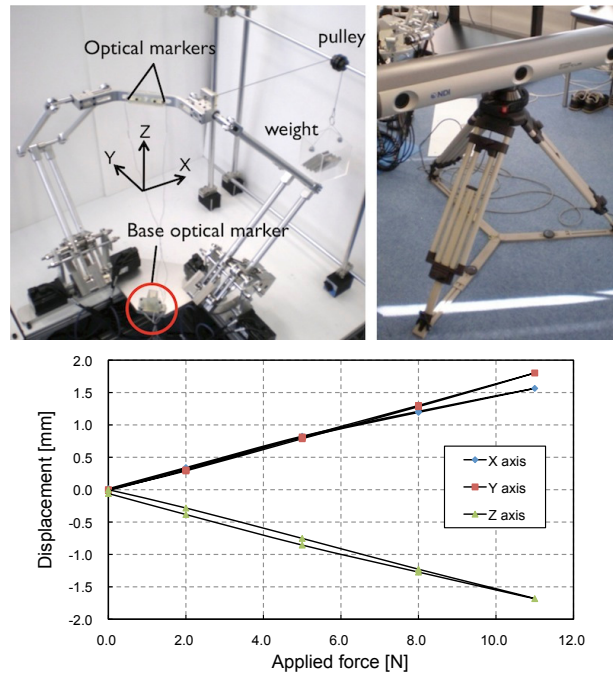
Fig. 8.   Experimental setup and results of the stiffness test

of the prototype in the X, Y, and Z directions are 7.03, 6.10, and 6.54 N/mm, respectively. In PHANTOM Premium 3.0[2] and Omega[8], the stiffnesses are 1.0 N/mm and 14.5 N/mm, respectively. The stiffness depends on the length of the arm and the implementation of the mechanism, for example. In addition, the working area of the DELTA-R prototype is over 10 times larger than that of Omega. Therefore, a simple comparison cannot be made. However, considering these conditions, the performance of the DELTA-R mechanism is advantageous with respect to stiffness.

C. Resistance force measurement in freehand motion

The resistance force is important for a haptic device in terms of backdrivability and inertia force, which are strongly related to operability. In this experiment, the resistance force was measured using a force sensor attached to an end-effector of the prototype.

1) Experimental setup: A force sensor (Nitta Corporation, IFS-50M31A25-I25) was attached to one of the end-effectors. This end-effector was held by the operator to measure the resistance force. Free-hand motion (XY plane) at a speed of approximately 150 mm/s was performed by the operator. An overview of the experimental setup and the trajectory of the end-effector are shown in the top panels of Fig. 9. In this experiment, no mechanical or software constraint was applied so that the device could be tested under the most commonly used condition. The data record indicates that the operator moved the end-effector to the prohibited direction approximately ±10 mm.

2) Experimental results: The bottom panel of Fig. 9 shows the experimental results. A resistance force was periodically observed in the freehand motion of the operator. The maximum resistance force was observed to be 3 N in the X direction.

Since the peak value was observed at the point at which the operator changed the direction of the end-effector, the primary cause of the resistance force is regarded as the inertia force. As described above, in this prototype, gravity is compensated by counterweights. These counterweights are considered to have increased the inertia force. In addition, the coulomb friction of the cables and the distortion of the mechanism can be affected in this result. The average force was 0.97 N in the X direction, 0.12 N in the Y direction, and -0.42 N in the Z direction.

D. Virtual sphere display

A virtual sphere was displayed on the prototype in order to test the general performance of the force display while using the prototype as a practical haptic device.

1) Experimental setup: In this test, a virtual sphere within a simple spring model (diameter: 200 mm, $K = 1.0$ N/mm) was displayed. For the case in which the operator attempted to move his/her hand outside the sphere, the force was displayed as a force wall to keep the end-effector inside the sphere. The experiment was conducted using 11 subjects (10 men and 1 woman) ranging in age from 21 to 35 years. All of the subjects were right-handed.

2) Experimental results: Figure 10 shows representative experimental results for the trajectory of the end-effector. The force was displayed when the operator moved outside the sphere. The trajectory of the end-effector clearly shows that the force was effectively displayed on the surface of the sphere. The results of a questionnaire given after the trial revealed that subjects clearly felt the smooth surface of the sphere. Therefore, the capability of the DELTA-R prototype was demonstrated qualitatively.
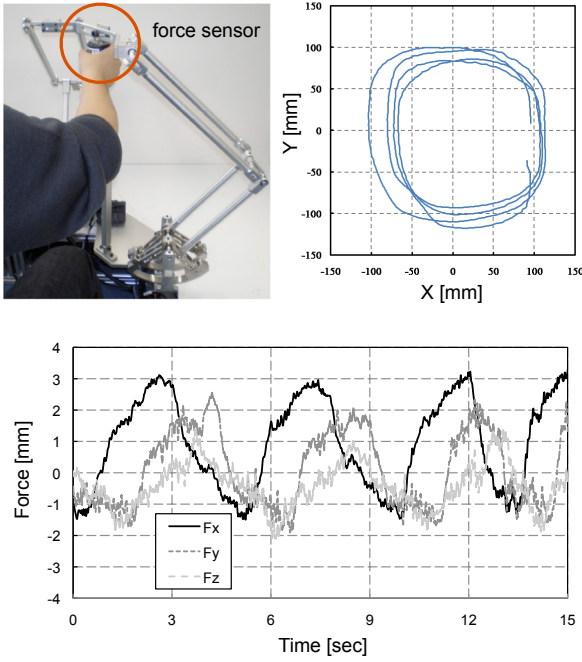
Fig. 9. Experimental setup and result of resistance force test
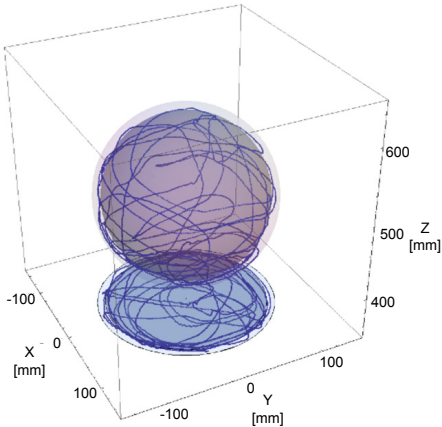
Fig. 10. Trajectory of the end-effector on a virtual sphere

VII. CONCLUSIONS

In the present paper, a new parallel mechanism, referred to herein as DELTA-R, was presented. This mechanism was designed for use in a haptic device. The structure of DELTA-R and its forward and inverse kinematic model and singularity points were described. Comparative analysis with a conventional parallel mechanism, i.e., DELTA, was presented. DELTA-R was demonstrated to realize a 40% smaller footprint and a 15% larger working area, as compared to DELTA. In addition, DELTA-R has an advantage in the working area distribution as a result of incorporating two arms. By aligning the arms and motors in a V shape, DELTA-R enables the operator to effectively access a large working area. As a kinematic analysis of DELTA-R and DELTA, force producibility analysis was carried out by introducing extremal forces to representative points over the working area. The

analysis results reveal that DELTA-R has a drawback with respect to force producibility for cases in which X and Y are negative. This drawback is caused by the spatial configuration of the DELTA-R mechanism. However, it was shown that this drawback can be overcome through proper mechanical design of the kinematics. A prototype haptic device incorporating the DELTA-R mechanism was evaluated. A force display test revealed an accurate force display capability of the prototype (0.15 N average error). The crosstalk of the output force (approximately 0.5 N in X-Y plane) was observed in the test, and this phenomenon was explained by the kinematic analysis. A stiffness test revealed that the prototype had relatively advantageous stiffness characteristic (6.56 N/mm in average of all axes) compared with conventional haptic devices. A qualitative test using a virtual sphere display revealed that the general performance of DELTA-R as a haptic device was good.

The redundant parallel mechanism provided a larger working area, a smaller footprint, and an improved working area distribution. Further investigation of redundancy for haptic performance is currently under way. Kumar et al. proposed a torque optimization method for a redundant parallel mechanism based on the manipulability parameter ω using a weighting factor[35]. This method can be effectively introduced for the purpose of singularity avoidance. However, since the DELTA-R mechanism has no singularity in the working area, this method can be used for torque optimization. In addition, only the mechanical characteristics of the prototype were tested in the present study. In the future, we intend to introduce a wire friction control approach and dynamic compensation to the prototype system.

APPENDIX
KINEMATICS OF DELTA-R

In general, robot statics can be denoted based on the virtual work principle as

$$\tau = \mathbf{J}^T \mathbf{F}, \tag{18}$$

where $\mathbf{J}$ is the Jacobian matrix, τ is the joint torque vector, and $\mathbf{F}$ is the display force vector. In DELTA-R, the Jacobian matrix $\mathbf{J}_i$ is a $\Re^{3 \times 4}$ matrix. In the kinematics of DELTA-R, the Jacobian $\mathbf{J}_i$ can be given in each arm ($i = 1, 2$). Although the values of $\mathbf{J}_1$ and $\mathbf{J}_2$ are identical in kinematic analysis, in order to compensate for errors that can occur as a result of backlash and play in the prototype, the mean of these values is used for the calculations:

$$\mathbf{J} = \frac{\mathbf{J}_1 + \mathbf{J}_2}{2}. \tag{19}$$

Therefore, the Jacobian matrix $\mathbf{J}$ can be obtained as

$$\mathbf{J} = \begin{bmatrix} \frac{\partial px_3}{\partial q1_1} & \frac{\partial px_3}{\partial q2_1} & \frac{\partial px_3}{\partial q1_2} & \frac{\partial px_3}{\partial q2_2} \\ \frac{\partial py_3}{\partial q1_1} & \frac{\partial py_3}{\partial q2_1} & \frac{\partial py_3}{\partial q1_2} & \frac{\partial py_3}{\partial q2_2} \\ \frac{\partial pz_3}{\partial q1_1} & \frac{\partial pz_3}{\partial q2_1} & \frac{\partial pz_3}{\partial q1_2} & \frac{\partial pz_3}{\partial q2_2} \end{bmatrix}, \tag{20}$$

where

$$\frac{\partial px_3}{\partial q1_1} = \frac{\frac{\partial px_1}{\partial q1_1} + \frac{\partial px_2}{\partial q1_1}}{2}, \qquad \frac{\partial px_3}{\partial q2_1} = \frac{\frac{\partial px_1}{\partial q2_1} + \frac{\partial px_2}{\partial q2_1}}{2},$$

$$\frac{\partial px_3}{\partial q1_2} = \frac{\frac{\partial px_1}{\partial q1_2} + \frac{\partial px_2}{\partial q1_2}}{2}, \qquad \frac{\partial px_3}{\partial q2_2} = \frac{\frac{\partial px_1}{\partial q2_2} + \frac{\partial px_2}{\partial q2_2}}{2},$$

$$\frac{\partial py_3}{\partial q1_1} = \frac{\frac{\partial py_1}{\partial q1_1} + \frac{\partial py_2}{\partial q1_1}}{2}, \qquad \frac{\partial py_3}{\partial q2_1} = \frac{\frac{\partial py_1}{\partial q2_1} + \frac{\partial py_2}{\partial q2_1}}{2},$$

$$\frac{\partial py_3}{\partial q1_2} = \frac{\frac{\partial py_1}{\partial q1_2} + \frac{\partial py_2}{\partial q1_2}}{2}, \qquad \frac{\partial py_3}{\partial q2_2} = \frac{\frac{\partial py_1}{\partial q2_2} + \frac{\partial py_2}{\partial q2_2}}{2},$$

$$\frac{\partial pz_3}{\partial q1_1} = \frac{\frac{\partial pz_1}{\partial q1_1} + \frac{\partial pz_2}{\partial q1_1}}{2}, \qquad \frac{\partial pz_3}{\partial q2_1} = \frac{\frac{\partial pz_1}{\partial q2_1} + \frac{\partial pz_2}{\partial q2_1}}{2},$$

$$\frac{\partial pz_3}{\partial q1_2} = \frac{\frac{\partial pz_1}{\partial q1_2} + \frac{\partial pz_2}{\partial q1_2}}{2}, \qquad \frac{\partial pz_3}{\partial q2_2} = \frac{\frac{\partial pz_1}{\partial q2_2} + \frac{\partial pz_2}{\partial q2_2}}{2},$$

$$\frac{\partial px_1}{\partial q1_1} = -L1C_{\theta1}S_{11} + \frac{2L2C_{21}C_{\theta1}S_{31}\frac{\partial u_1}{\partial q1_1}}{1+u_1^2} + \frac{2L2C_{31}S_{\theta1}\frac{\partial u_1}{\partial q1_1}}{1+u_1^2},$$

$$\frac{\partial px_1}{\partial q2_1} = L2C_{31}C_{\theta1}S_{21} + \frac{2L2C_{21}C_{\theta1}S_{31}\frac{\partial u_1}{\partial q2_1}}{1+u_1^2} + \frac{2L2C_{31}S_{\theta1}\frac{\partial u_1}{\partial q2_1}}{1+u_1^2},$$

$$\frac{\partial px_1}{\partial q1_2} = \frac{2L2C_{21}C_{\theta1}S_{31}\frac{\partial u_1}{\partial q1_2}}{1+u_1^2} + \frac{2L2C_{31}S_{\theta1}\frac{\partial u_1}{\partial q1_2}}{1+u_1^2},$$

$$\frac{\partial px_1}{\partial q2_2} = \frac{2L2C_{21}C_{\theta1}S_{31}\frac{\partial u_1}{\partial q2_2}}{1+u_1^2} + \frac{2L2C_{31}S_{\theta1}\frac{\partial u_1}{\partial q2_2}}{1+u_1^2},$$

$$\frac{\partial px_2}{\partial q1_1} = \frac{2L2C_{22}C_{\theta2}S_{32}\frac{\partial u_2}{\partial q1_1}}{1+u_2^2} + \frac{2L2C_{32}S_{\theta2}\frac{\partial u_2}{\partial q1_1}}{1+u_2^2},$$

$$\frac{\partial px_2}{\partial q2_1} = \frac{2L2C_{22}C_{\theta2}S_{32}\frac{\partial u_2}{\partial q2_1}}{1+u_2^2} + \frac{2L2C_{32}S_{\theta2}\frac{\partial u_2}{\partial q2_1}}{1+u_2^2},$$

$$\frac{\partial px_2}{\partial q1_2} = -L1C_{\theta2}S_{12} + \frac{2L2C_{22}C_{\theta2}S_{32}\frac{\partial u_2}{\partial q1_2}}{1+u_2^2} + \frac{2L2C_{32}S_{\theta2}\frac{\partial u_2}{\partial q1_2}}{1+u_2^2},$$

$$\frac{\partial px_2}{\partial q2_2} = L2C_{32}C_{\theta2}S_{22} + \frac{2L2C_{22}C_{\theta2}S_{32}\frac{\partial u_2}{\partial q2_2}}{1+u_2^2} + \frac{2L2C_{32}S_{\theta2}\frac{\partial u_2}{\partial q2_2}}{1+u_2^2},$$

$$\frac{\partial py_1}{\partial q1_1} = -L1S_{11}S_{\theta1} - \frac{2L2C_{31}C_{\theta1}\frac{\partial u_1}{\partial q1_1}}{1+u_1^2} + \frac{2L2C_{21}S_{31}S_{\theta1}\frac{\partial u_1}{\partial q1_1}}{1+u_1^2},$$

$$\frac{\partial py_1}{\partial q2_1} = L2C_{31}S_{21}S_{\theta1} - \frac{2L2C_{31}C_{\theta1}\frac{\partial u_1}{\partial q2_1}}{1+u_1^2} + \frac{2L2C_{21}S_{31}S_{\theta1}\frac{\partial u_1}{\partial q2_1}}{1+u_1^2},$$

$$\frac{\partial py_1}{\partial q1_2} = -\frac{2L2C_{31}C_{\theta1}\frac{\partial u_1}{\partial q1_2}}{1+u_1^2} + \frac{2L2C_{21}S_{31}S_{\theta1}\frac{\partial u_1}{\partial q1_2}}{1+u_1^2},$$

$$\frac{\partial py_1}{\partial q2_2} = -\frac{2L2C_{31}C_{\theta1}\frac{\partial u_1}{\partial q2_2}}{1+u_1^2} + \frac{2L2C_{21}S_{31}S_{\theta1}\frac{\partial u_1}{\partial q2_2}}{1+u_1^2},$$

$$\frac{\partial py_2}{\partial q1_1} = -\frac{2L2C_{32}C_{\theta2}\frac{\partial u_2}{\partial q1_1}}{1+u_2^2} + \frac{2L2C_{22}S_{32}S_{\theta2}\frac{\partial u_2}{\partial q1_1}}{1+u_2^2},$$

$$\frac{\partial py_2}{\partial q2_1} = -\frac{2L2C_{32}C_{\theta2}\frac{\partial u_2}{\partial q2_1}}{1+u_2^2} + \frac{2L2C_{22}S_{32}S_{\theta2}\frac{\partial u_2}{\partial q2_1}}{1+u_2^2},$$

$$\frac{\partial py_2}{\partial q1_2} = -L1S_{12}S_{\theta2} - \frac{2L2C_{32}C_{\theta2}\frac{\partial u_2}{\partial q1_2}}{1+u_2^2} + \frac{2L2C_{22}S_{32}S_{\theta2}\frac{\partial u_2}{\partial q1_2}}{1+u_2^2},$$

$$\frac{\partial py_2}{\partial q2_2} = L2C_{32}S_{21}S_{\theta2} - \frac{2L2C_{32}C_{\theta2}\frac{\partial u_2}{\partial q2_2}}{1+u_2^2} + \frac{2L2C_{22}S_{32}S_{\theta2}\frac{\partial u_2}{\partial q2_2}}{1+u_2^2},$$

$$\frac{\partial pz_1}{\partial q1_1} = L1C_{11} - \frac{2L2S_{31}S_{21}\frac{\partial u_1}{\partial q1_1}}{1+u_1^2},$$

$$\frac{\partial pz_1}{\partial q2_1} = L2C_{31}C_{21} - \frac{2L2S_{31}S_{21}\frac{\partial u_1}{\partial q2_1}}{1+u_1^2},$$

$$\frac{\partial pz_1}{\partial q1_2} = -\frac{2L2S_{31}S_{21}\frac{\partial u_1}{\partial q1_2}}{1+u_1^2},$$

$$\frac{\partial pz_1}{\partial q2_2} = -\frac{2L2S_{31}S_{21}\frac{\partial u_1}{\partial q2_2}}{1+u_1^2},$$

$$\frac{\partial pz_2}{\partial q1_1} = -\frac{2L2S_{32}S_{22}\frac{\partial u_2}{\partial q1_1}}{1+u_2^2},$$

$$\frac{\partial pz_2}{\partial q2_1} = -\frac{2L2S_{32}S_{22}\frac{\partial u_2}{\partial q2_1}}{1+u_2^2},$$

$$\frac{\partial pz_2}{\partial q1_2} = L1C_{12} - \frac{2L2S_{32}S_{22}\frac{\partial u_2}{\partial q1_2}}{1+u_2^2},$$

$$\frac{\partial pz_2}{\partial q2_2} = L2C_{32}C_{22} - \frac{2L2S_{32}S_{22}\frac{\partial u_2}{\partial q2_2}}{1+u_2^2},$$

$$\frac{\partial A_i}{\partial q1_i} = -L1S_{1i}C_{\theta i}, \qquad \frac{\partial B_i}{\partial q1_i} = -L1S_{1i}S_{\theta i},$$

$$\frac{\partial C_i}{\partial q2_i} = -L2C_{2i}C_{\theta i}, \qquad \frac{\partial D_i}{\partial q2_i} = -L2C_{2i}S_{\theta i},$$

$$\frac{\partial E_i}{\partial q1_1} = L1C_{11}, \qquad \frac{\partial E_i}{\partial q1_2} = -L1C_{12},$$

$$\frac{\partial E_i}{\partial q2_2} = -L2C_{2i}, \qquad \frac{\partial F_i}{\partial q1_1} = L1C_{11},$$

$$\frac{\partial F_i}{\partial q1_2} = -L1C_{12}, \qquad \frac{\partial F_i}{\partial q2_1} = L2C_{2i},$$

$$\frac{\partial H_1}{\partial q1_1} = \left(L2\frac{\partial A_1}{\partial q1_1} + \frac{C_2\frac{\partial E_1}{q1_1}}{S_{22}}\right)C_{\theta2} + \left(L2\frac{\partial B_1}{\partial q1_1} + \frac{D_2\frac{\partial E_1}{q1_1}}{S_{22}}\right)S_{\theta2},$$

$$\frac{\partial H_1}{\partial q2_1} = \left(L2\frac{\partial C_1}{\partial q2_1} + \frac{C_2\frac{\partial E_1}{q2_1}}{S_{22}}\right)C_{\theta2} + \left(L2\frac{\partial D_1}{\partial q2_1} + \frac{D_2\frac{\partial E_1}{q2_1}}{S_{22}}\right)S_{\theta2},$$

$$\frac{\partial H_1}{\partial q1_2} = \left(-L2\frac{\partial A_2}{\partial q1_2} + \frac{C_2\frac{\partial E_1}{q1_2}}{S_{22}}\right)C_{\theta2} + \left(-L2\frac{\partial B_1}{\partial q1_1} + \frac{D_2\frac{\partial E_1}{q1_2}}{S_{22}}\right)S_{\theta2},$$

$$\frac{\partial H_1}{\partial q2_2} = \left(-\frac{C_{22}}{S_{22}}\frac{C_2E_1}{S_{22}} + \frac{E_1\frac{\partial C_2}{q22}}{S_{22}}\right)C_{\theta2} + \left(-\frac{C_{22}}{S_{22}}\frac{D_2E_1}{S_{22}} + \frac{E_1\frac{\partial D_2}{q22}}{S_{22}}\right)C_{\theta2},$$

$$\frac{\partial H_2}{\partial q1_1} = \left(L2\frac{\partial A_1}{\partial q1_1} + \frac{C_1\frac{\partial F_2}{q1_1}}{S_{21}}\right)C_{\theta1} + \left(L2\frac{\partial B_1}{\partial q1_1} + \frac{D_1\frac{\partial F_2}{q1_1}}{S_{21}}\right)S_{\theta1},$$

$$\frac{\partial H_2}{\partial q2_1} = \left(-\frac{C_{21}}{S_{21}}\frac{C_1F_2}{S_{21}} + \frac{F_2\frac{\partial C_1}{q2_1}}{S_{21}}\right)C_{\theta1} + \left(-\frac{C_{21}}{S_{21}}\frac{D_1F_2}{S_{21}} + \frac{F_2\frac{\partial D_1}{q2_1}}{S_{21}}\right)C_{\theta1},$$

$$\frac{\partial H_2}{\partial q1_2} = \left(-L2\frac{\partial A_2}{\partial q1_1} + \frac{C_1\frac{\partial F_2}{q1_2}}{S_{21}}\right)C_{\theta1} + \left(L2\frac{\partial B_1}{\partial q1_1} + \frac{D_1\frac{\partial F_2}{q1_2}}{S_{21}}\right)S_{\theta1},$$

$$\frac{\partial H_2}{\partial q2_2} = \left(-L2\frac{\partial C_2}{\partial q2_2} + \frac{C_1\frac{\partial F_2}{q2_2}}{S_{21}}\right)C_{\theta1} + \left(-L2\frac{\partial D_2}{\partial q2_2} + \frac{D_1\frac{\partial F_2}{q2_2}}{S_{21}}\right)S_{\theta1},$$

$$\frac{\partial I_1}{\partial q1_1} = \left(L2\frac{\partial A_1}{\partial q1_1} + \frac{C_2\frac{\partial F_1}{q1_1}}{S_{22}}\right)C_{\theta2} + \left(L2\frac{\partial B_1}{\partial q1_1} + \frac{D_2\frac{\partial F_1}{q1_1}}{S_{22}}\right)S_{\theta2},$$

$$\frac{\partial I_1}{\partial q2_1} = \left(-L2\frac{\partial A_2}{\partial q1_2} + \frac{C_2\frac{\partial F_1}{q1_2}}{S_{22}}\right)C_{\theta2} + \left(-L2\frac{\partial B_2}{\partial q1_2} + \frac{D_2\frac{\partial F_1}{q1_2}}{S_{22}}\right)S_{\theta2},$$

$$\frac{\partial I_1}{\partial q1_2} = \left(-L2\frac{\partial C_1}{\partial q2_1} + \frac{C_2\frac{\partial F_1}{q2_1}}{S_{22}}\right)C_{\theta2} + \left(-L2\frac{\partial D_1}{\partial qD_1} + \frac{D_2\frac{\partial F_1}{q2_1}}{S_{22}}\right)S_{\theta2},$$

$$\frac{\partial I_1}{\partial q2_2} = \left(-\frac{C_{22}}{S_{22}}\frac{C_2F_1}{S_{22}} + \frac{F_1\frac{\partial C_2}{q22}}{S_{22}}\right)C_{\theta2} + \left(-\frac{C_{22}}{S_{22}}\frac{D_2F_1}{S_{22}} + \frac{F_1\frac{\partial D_2}{q22}}{S_{22}}\right)C_{\theta2},$$

$$\frac{\partial I_2}{\partial q1_1} = \left(L2\frac{\partial A_1}{\partial q1_1} + \frac{C_1\frac{\partial E_2}{q1_1}}{S_{21}}\right)C_{\theta1} + \left(L2\frac{\partial B_1}{\partial q1_1} + \frac{D_1\frac{\partial E_2}{q1_1}}{S_{21}}\right)S_{\theta1},$$

$$\frac{\partial I_2}{\partial q2_1} = \left(-\frac{C_{21}}{S_{21}}\frac{C_1E_2}{S_{21}} + \frac{E_2\frac{\partial C_1}{q2_1}}{S_{21}}\right)C_{\theta1} + \left(-\frac{C_{21}}{S_{21}}\frac{D_1E_2}{S_{21}} + \frac{E_2\frac{\partial D_1}{q2_1}}{S_{21}}\right)C_{\theta1},$$

$$\frac{\partial I_2}{\partial q1_2} = \left(-L2\frac{\partial A_2}{\partial q1_2} + \frac{C_1\frac{\partial E_2}{q1_2}}{S_{21}}\right)C_{\theta1} + \left(-L2\frac{\partial B_1}{\partial q1_2} + \frac{D_1\frac{\partial E_2}{q1_2}}{S_{21}}\right)S_{\theta1},$$

$$\frac{\partial I_2}{\partial q2_2} = \left(L2\frac{\partial C_1}{\partial q2_1} + \frac{C_1\frac{\partial E_2}{q2_2}}{S_{21}}\right)C_{\theta1} + \left(L2\frac{\partial D_1}{\partial qD_1} + \frac{D_1\frac{\partial E_2}{q2_2}}{S_{21}}\right)S_{\theta1},$$

$$\frac{\partial u_i}{\partial q1_1} = \frac{\left(-G_i - \sqrt{G_i^2 - 4H_iI_i}\right)\frac{\partial H_i}{\partial q1_1}}{2H_i^2} - \frac{-4I_i\frac{\partial H_i}{\partial q1_1} - 4H_i\frac{\partial I_i}{\partial q1_1}}{4H_i\sqrt{G_i^2 - 4H_i^2}},$$

$$\frac{\partial u_i}{\partial q2_1} = \frac{\left(-G_i - \sqrt{G_i^2 - 4H_iI_i}\right)\frac{\partial H_i}{\partial q2_1}}{2H_i^2} - \frac{-4I_i\frac{\partial H_i}{\partial q2_1} - 4H_i\frac{\partial I_i}{\partial q2_1}}{4H_i\sqrt{G_i^2 - 4H_iI_i}},$$

$$\frac{\partial u_i}{\partial q1_2} = \frac{\left(-G_i - \sqrt{G_i^2 - 4H_iI_i}\right)\frac{\partial H_i}{\partial q1_2}}{2H_i^2} - \frac{-4I_i\frac{\partial H_i}{\partial q1_2} - 4H_i\frac{\partial I_i}{\partial q1_2}}{4H_i\sqrt{G_i^2 - 4H_iI_i}},$$

$$\frac{\partial u_i}{\partial q2_2} = \frac{\left(-G_i - \sqrt{G_i^2 - 4H_iI_i}\right)\frac{\partial H_i}{\partial q2_2}}{2H_i^2} - \frac{-4I_i\frac{\partial H_i}{\partial q2_2} - 4H_i\frac{\partial I_i}{\partial q2_2}}{4H_i\sqrt{G_i^2 - 4H_iI_i}}.$$

Joint torque vector τ is a $\Re^{4\times1}$ matrix, and the display force vector $\mathbf{F}$ is a $\Re^{3\times1}$ matrix and can be given as follows:

$$\tau = \begin{bmatrix} \tau_{11} & \tau_{21} & \tau_{12} & \tau_{22} \end{bmatrix}^T, \qquad (21)$$

$$\mathbf{F} = \begin{bmatrix} F_x & F_y & F_z \end{bmatrix}^T. \qquad (22)$$

Thus, for displaying force on the prototype, the required torque τ can be given in terms of the Jacobian matrix $\mathbf{J}$ and the display force vector $\mathbf{F}$ as follows:

$$\begin{pmatrix} \tau_{11} \\ \tau_{21} \\ \tau_{12} \\ \tau_{22} \end{pmatrix} = \begin{pmatrix} \frac{\partial px_3}{\partial q1_1}F_x + \frac{\partial py_3}{\partial q1_1}F_y + \frac{\partial pz_3}{\partial q1_1}F_z \\ \frac{\partial px_3}{\partial q2_1}F_x + \frac{\partial py_3}{\partial q2_1}F_y + \frac{\partial pz_3}{\partial q2_1}F_z \\ \frac{\partial px_3}{\partial q1_2}F_x + \frac{\partial py_3}{\partial q1_2}F_y + \frac{\partial pz_3}{\partial q1_2}F_z \\ \frac{\partial px_3}{\partial q2_2}F_x + \frac{\partial py_3}{\partial q2_2}F_y + \frac{\partial pz_3}{\partial q2_2}F_z \end{pmatrix}. \qquad (23)$$

ACKNOWLEDGMENTS

REFERENCES

[1] J.P. Merlet, "Parallel Robots Second Edition,", Springer, ISBN 1-4020-4132-2, 2006.

[2] SensAble Technologies: http://www.sensable.com/

[3] MPB Technologies: http://www.mpb-technologies.ca/

[4] Haption: http://www.haption.com/site/index.html

[5] Immersion: http://www.immersion.com/

[6] R. Clavel, "Conception d'un robot parallèle rapide à 4 degrés de liberté," Ph.D. Thesis, EPFL, Lausanne, 1991. No.925.

[7] R. Clavel, "Une Nouvelle Structure de Manipulateur Paralléle pour la Robotique Légère," Automatique-Productique Informatique Industrielle, vol.23, pp.501-519, 1989.

[8] Force Dimension: http://www.forcedimension.com/

[9] Novint Technologies: http://home.novint.com/

[10] HapticMaster: http://intron.kz.tsukuba.ac.jp/vrlab_web/hapticmaster/hapticmaster_e.html

[11] H.Iwata,"Pen-based Haptic Virtual Environment," IEEE Virtual Reality Annual International Symposium, pp.287-292, 1993.

[12] Quanser: http://www.quanser.com/choice.asp

[13] H. Iwata,"Artificial Reality with Force-feedback: Development of Desktop Virtual Space with Compact Master Manipulator," Computer Graphics, Vol.24, No.4, pp.165-170, 1990.

[14] T. Asano, H. Yano and H. Iwata,"Basic Technology of Simulation System for Laparoscopic Surgery in Virtual Environment with Force Display," Medicine Meets Virtual Reality, Global Healthcare Grid, Studies in Health Technology and Informatics, IOS Press, vol.39, pp.207-215, 1997.

[15] L. Birglen, "SHaDe, A New 3-DOF Haptic Device," IEEE Trans. on Robotics and Automation, Vol. 18, NO. 2, pp.166-175, APRIL 2002.

[16] R. Clavel et al., "The PantoScope: A Spherical Remote-Center-of-Motion Parallel Manipulator for Force Reflection," Proc. of IEEE Int. Conf. on Robotics and Automation 1997, pp.718-723, New Mexico, 1997.

[17] Mentice: http://www.mentice.com/

[18] B.D.Adelstein, P.Ho, H.Kazerooni. Kinematic Design of a Three Degree of Freedom Parallel Hand Controller Mechanism. ASME Dynamic System and Control Division, DSC-vol.58, pp. 539-546, 1996.

[19] D. Chablet, P. Wenger. A Six Degree-Of-Freedom Haptic Device Baced On The Orthoglide And A Hybrid Agile Eye. IDETC 2006, 30th Mechanism & Robotics Conference(MR), September 10-13, 2006, Philadelphia, USA.

[20] L. Buoguila, Y.Cai, M.Sato,"New Haptic Device For Human Scale Virtual Environment Scalable-SPIDAR," Proc. of Int. Conf. on Artificial Reality and Telexistence, pp.93-98, 1997.

[21] CyVerse: http://www.cyverse.co.jp/

[22] Mimic Technologies: http://www.mimic.ws/

[23] S. Kawamura and K. Ito,"A New Type of Master Robot for Teleoperation Using A Radial Wire Drive System," Proceedings of the IEEE International Conference on Intelligent Robots and Systems pp.55-60, 1993.

[24] R.J. Adams, D. Klowden, B. Hannaford, "Stable Haptic Interaction using the Excalibur Force Display," Proc. of the IEEE Int. Conf. on Robotics and Automation, pp. 770-775,2000.

[25] C. Bonivento, A. Eusebi, C. Melchiorri, M. Montanari, G. Vassura,"WireMan:A Portable Wire Manipulator for Touch-Rendering of Bas-Relief Virtual Surfaces," Proc. of the Int. Conf. on Advanced Robotics, pp. 13-18, 1997.

[26] N. Hirose, K. Hirota, T. Ogi, H. Yano, N. Kakehi, M. Saito, M.Nakashige,"HapticGEAR: the development of a wearable force display system for immersive projection displays," Proc. of the IEEE Int. Conf. on Virtual Reality, pp.123-129, 2001.

[27] J.V. Zitzewitz, G. Rauter, R. Steiner, A. Brunschweiler, and R. Riener,"A versatile wire robot concept as a haptic interface for sport simulation," Proc. of the IEEE Int. Conf. on Intelligent Robots and Systems, pp.313-318, 2009.

[28] Moog FCS Robotics: http://www.moog.com/simulationandtesting/

[29] M. Ueberle and M. Buss, "Design, control, and evaluation of a new 6 DOF haptic device," Proc. of the Int. Conf. on Intelligent Robots and System, pp.2949-2954:3, 2002.

[30] M. Ueberle, N. Mock, "VISHARD10, a Novel Hyper-Redundant Haptic Interface," Proc. of the Int. Symposium on Haptic Interfaces for Virtual Environment and Teleoperator Systems, pp.58-65, 2004.

[31] Y. Tsumaki, H. Naruse, D.N. Nenchev and M. Uchiyama, "Design of a Compact 6-DOF Haptic Interface," Proc. of Int. Conf. of Robotics and Automation, pp.2580-2585, 1998.

[32] L.W. Tsai, "Multi-degree-of-freedom mechanisms for machine tools and like," U.S. Patent, no.5656905, 1995.

[33] M. Ouerfelli and V.Kuma, "Optimization of a Spherical Five-Bar Parallel Drive Linkage," Trans. of the ASME, J. of Mechanical Design, vol.116, March, pp.166-173, 1994.

[34] Optotrak Certus: http://www.ndigital.com/medical/certus.php

[35] V.R. Kumar and J.F. Gardner, "Kinematics of Redundantly Actuated Closed Kinematic Chains," IEEE Trans. on Robotics and Automation, 6(2), pp.269-274, 1990.

[36] J. Arata, H. Kondo, M. Sakaguchi H. Fujoimoto, "Development of a Haptic Device "DELTA-4" using Parallel Link Mechanism," Proc. of Int. Conf. Robotics and Automation, pp.294-300, 2009.

[37] J. Arata, H. Kondo, M. Sakaguchi, H. Fujoimoto, "A haptic device DELTA-4: kinematics and its analysis," Proc. of world Haptics, pp.452-457, 2009.

Jumpei Arata (M'06) received an undergraduate degree in mechanical control systems from Shibaura Institute of Technology, Japan in 1997 and a master's degree in mechanical engineering from Shibaura Institute of Technology, Japan in 2000, and a Ph.D. degree in mechanical engineering from the University of Tokyo, Japan in 2004. During 1998 and 2001, he spent two years in total at the Swiss Federal Institute of Technology Lausanne, Switzerland, granted by an international exchange program and an Swiss Federal Scholarship. In these period, He was an half assistant and an half student. He is currently an assistant professor at the Nagoya Institute of Technology, Japan. His current research interests include parallel mechanisms, flexible mechanisms, haptic devices, medical robotics. He is a member of the IEEE Robotics and Automation Society, the Robotics Society of Japan, the Japan Society of Mechanical Engineers, the Japan Society of Computer Aided Surgery, and the International Society of Computer Aided Surgery.

Hiroyuki Kondo received an undergraduate degree in mechanical engineering from Tokai University, Japan in 2007 and a master's degree in mechanical engineering from Nagoya Institute of Technology, Japan in 2009. His research interests for his master's degree included mechanical design and haptic devices.

Norio Ikedo received an undergraduate degree in mechanical engineering from Gifu University, Japan in 2009. He is currently a student in the master's degree program in mechanical engineering at the Nagoya Institute of Technology, Japan. His research interests include kinematic modeling and haptic devices.

Hideo Fujimoto received an undergraduate degree and Ph.D. degree in mechanical engineering from Nagoya University, Nagoya, Japan in 1970 and 1982, respectively. He is currently a professor at the Graduate School, Nagoya Institute of Technology, Nagoya, Japan, where he is also the Director of the Quality Innovation Techno-Center. His current research interests include medical engineering, haptic engineering, and robotics. He is a Fellow and a Councilor of the Japan Society of Mechanical Engineers and the Chairperson of Aichi Prefecture Manufacturing Personnel Training Meeting. He was a member of the Committee on Cultural Resources of the Council for Science and Technology of the Ministry of Education, Culture, Sports, Science and Technology of Japan and the President of the Scheduling Society of Japan. He was the recipient of the Best Paper Award for a paper presented at the Japan-USA Flexible Automation Symposium 2000, the Best Paper Award at the 6th Robotics Symposium, the Contribution Award from the System Integration Section, Society of Instrument and Control Engineers, and the Great Contribution Award from the Production System Section and the Japan Society of Mechanical Engineers in 2002.